Enhanced weathering of glacial rock flour drives coupled inorganic and organic carbon sequestration in a five-year field experiment

Christiana Dietzen[1], Malgorzata Rizzi[1], Tim Jesper Suhrhoff[2,3], Minik Thorleif Rosing[1]

[1] Globe Institute, University of Copenhagen, 1350 Copenhagen, Denmark

[2] Yale Center for Natural Carbon Capture, Yale University, New Haven, CT, 06511, USA

[3] Department of Earth & Planetary Sciences, Yale University, New Haven, CT, 06511, USA

Correspondence to: Christiana Dietzen (christiana.dietzen@sund.ku.dk)

Abstract. Enhanced rock weathering (ERW) has been proposed as a scalable carbon dioxide removal strategy, yet long-term field-based constraints on weathering rates and associated carbon sequestration remain limited. Here, we present a five-year field assessment of Greenlandic glacial rock flour (GRF) applied at 50 t ha^{-1} to a sandy agricultural soil in Denmark. Using a soil mass balance approach, based on depletion of Mg which provided the most tightly constrained weathering signal, we estimate that at least 56% of the applied GRF dissolved over five years. Initial uptake of CO_2 via ERW is estimated at 3.2-4.9 t CO_2 ha^{-1} when accounting for carbonate speciation in the acidic soil solution, with the potential for further gains if complete downstream transport of weathering products and subsequent re-equilibration with the more alkaline marine carbonate system is assumed. In addition to inorganic carbon removal, GRF-treated plots exhibited significantly higher soil organic carbon stocks, equivalent to the storage of an additional 18.3 t CO_2 ha^{-1}. These results demonstrate substantial weathering and carbon sequestration over five years under field conditions in a temperate climate and suggest that both inorganic and organic carbon dynamics contribute meaningfully to the overall climate impact of ERW of GRF. The findings provide rare multi-year field constraints on ERW performance and underscore the importance of robust measurements for quantifying carbon removal in agricultural systems, representing the first implementation of mass balance methods within the framework of a randomized block design.

1. Introduction

Enhanced rock weathering (ERW) has emerged as a promising carbon dioxide removal (CDR) strategy that removes atmospheric CO_2 by accelerating the natural weathering of silicate minerals while simultaneously delivering agronomic co-benefits (Beerling et al., 2018; Hartmann et al., 2013). By enhancing the dissolution of silicate minerals in soils, ERW releases base cations and generates alkalinity, promoting the formation of dissolved inorganic carbon that may ultimately be transported to the ocean and stored for thousands of years (Köhler et al., 2010; Renforth and Henderson, 2017).

Despite growing interest in ERW, long-term field-based estimates of weathering rates of applied silicate minerals under realistic agricultural conditions remain limited (Buma et al., 2026). Most estimates are derived from laboratory experiments, short-term mesocosm studies, reactive transport modelling, or relatively short field trials, which cannot fully capture the hydrological variability, plant-soil interactions, and seasonal leaching dynamics that govern weathering in the field (Beerling et al., 2024; Dupla et al., 2025; Larkin et al., 2022). Because weathering rates are expected to decrease as reactive surface area is depleted (Brantley, 2025; Calabrese et al., 2021; Power et al., 2025), longer-term field assessments are critical for constraining realistic weathering rates and associated carbon sequestration.

Among the materials investigated for ERW, Greenlandic glacial rock flour has gained attention due to its extremely fine particle size, high specific surface area, and compositional homogeneity (Sarkar, 2021). Because it is naturally fine-grained, it can be deployed without the energy-intensive grinding typically required for conventional ERW feedstocks. Glacial rock flour (GRF) has been shown to be an effective alternative to traditional ERW materials for both carbon capture and crop yield improvement (Dietzen and Rosing, 2023; Gunnarsen et al., 2023; Obour et al., 2024; Oppong Danso et al., 2025; Tingey et al., 2025). In previous work, we estimated that 7.9% of GRF applied to an organic farm in Denmark weathered over approximately three years based on repeated measurements of exchangeable Mg (Dietzen and Rosing, 2023). Because this approach relied on discrete measurements of the exchangeable pool, weathering-derived cations exported between sampling events may not be captured, potentially underestimating cumulative dissolution, particularly in rapidly draining sandy soils (Huang and Hartemink, 2020).

To address these limitations, we reevaluated the weathering of GRF five years after its application using soil mass balance ("SOMBA") methods developed since our initial analysis (Suhrhoff et al., 2025). These approaches, sometimes referred to as the "TiCAT" method (Reershemius et al., 2023; Suhrhoff et al., 2024), use immobile tracers such as Ti to quantify the contribution of applied material to the sampled soil volume. By comparing the inferred soil cation concentrations before weathering to observed concentrations at the time of sampling, SOMBA provides a means of distinguishing time-integrated loss of feedstock attributable to weathering from other losses. To date, these methods have not yet been applied within randomized block designs typical of agricultural field experiments, which can help mitigate within-site soil heterogeneity that may otherwise limit the reliability of SOMBA-based estimates of weathering. In this study, we present a framework for integrating SOMBA methods into randomized block field experiments to enable more robust estimation of weathering in ERW trials.

In addition to uncertainties in bicarbonate generation, the overall carbon balance of ERW systems remains incompletely understood because potential effects on soil organic carbon (SOC) are rarely integrated into CDR assessments (Bijma et al., 2026; Vicca et al., 2022). Though research on changes in organic carbon fluxes in the context of ERW is limited, insights from liming studies (Wang et al., 2021; Zhang et al., 2022) may provide a useful analogue for understanding SOC responses to ERW, as both processes modify soil acidity and increase base cation availability. Liming experiments frequently report an initial pulse of SOC mineralization following increases in soil pH, but longer-term responses can include enhanced plant productivity, as observed in the first year of this experiment (Gunnarsen et al., 2023), greater belowground carbon inputs, and increased stabilization of microbial residues in mineral-associated organic matter (MAOM) (Paradelo et al., 2015). Consistent with this balance between enhanced carbon inputs and stimulated microbial turnover, experimental studies of silicate amendments have thus far reported both increases and decreases in SOC (Suhrhoff et al., 2026a; Xu et al., 2025), highlighting the strong dependence of SOC responses on site conditions, mineralogy, and timescale and emphasizing the need for multi-year field observations. Among the potential mechanisms influencing SOC dynamics under ERW, organo-mineral interactions may be particularly important for fine-grained materials such as GRF, which introduce additional reactive mineral surfaces that could promote SOC stabilization. Microbial processing of plant-derived inputs produces organic compounds that can bind to reactive mineral surfaces through sorption and organo-mineral interactions, forming MAOM that is less prone to rapid decomposition (Basile-Doelsch et al., 2020; Kleber et al., 2021). Such processes may be particularly relevant in coarse-textured sandy soils, which typically contain low clay fractions, limited abundance of reactive secondary minerals, and correspondingly low specific surface area, constraining MAOM formation by limiting the availability of mineral surfaces capable of stabilizing organic compounds (Georgiou et al., 2025; Six et al., 2002). In such systems, the addition of finely ground silicate material could disproportionately increase mineral surface area relative to the native soil matrix and potentially enhance opportunities for organo-mineral stabilization.

Despite these hypothesized mechanisms, the net effect of ERW on SOC remains poorly constrained under field conditions, particularly over multi-year timescales and alongside measurements of inorganic CDR. Here, we reassess the weathering of GRF five years after application at the Vojens field site using the SOMBA soil mass balance framework, representing the first application of SOMBA within a replicated, randomized block design field experiment. We quantify cumulative GRF dissolution and associated inorganic CO2 sequestration while simultaneously assessing changes in total and fractionated SOC. Together, these measurements allow us to evaluate both inorganic and organic components of the carbon response to GRF under temperate agricultural conditions.

2. Materials and Methods

2.1 Study Site and Experimental Design

The study was established in 2019 on an organic farm in Vojens, Denmark (55.204556, 9.265528) (Dietzen and Rosing, 2023; Gunnarsen et al., 2023). The soils at the site are classified as Cambic Arenosols with a loamy sand texture, formed from glacial outwash sands (GEUS, 2022). These soils have a relatively low cation exchange capacity of 7.16 $cmol_c\ kg^{-1}$ and high base saturation (~90%) (Dietzen et al., 2022). The mean annual temperature during the years in which the experiment took place (2019-2024) was 9.4° C and the mean annual precipitation was 968 mm yr^{-1} (DMI, 2026). Treatments included GRF applied at 10 and 50 t ha^{-1} along with a control arranged as a randomized block design with four replicates, but only the 50 t ha^{-1} treatments were analyzed in this study. The 10 t ha^{-1} treatment was excluded from this re-analysis due to the limited sensitivity of the SOMBA method at lower application rates (Suhrhoff et al., 2024). GRF treatments were applied by hand to 1 m^2 quadrants to ensure uniform application rates across the 3 x 20 m plots. Full details of the experimental setup, including additional treatments not relevant to this analysis, can be found in Gunnarsen et al. (2023).

2.2 Glacial rock flour

The glacial rock flour (GRF) used in this experiment was sourced from the Ilulialik locality in Greenland (64.782806, -50.625806). The material has an extremely fine grain size (d_{50} = 2.6 μm) and a high specific surface area (BET SSA = 19.6 $m^2\ g^{-1}$; as reported in Sarkar, 2021). Mineralogically, the material is primarily derived from felsic bedrock and consists of approximately 27.4% biotite, 18.6% oligoclase/andesine, 14.6% amphibole, 14.1% anorthite, 10.5% quartz, 4.3% Fe-oxide, 2.8% K-feldspar, and 2.4% muscovite, as determined by scanning electron microscopy (ZEISS Sigma 300VP Field Emission SEM; Geological Survey of Denmark and Greenland). Further information regarding the material can be found in Dietzen & Rosing (2023) and Sarkar (2021).

2.3 Soil Sampling and Analysis

Soil samples were collected on March 20th, 2024, approximately five years after the GRF was originally applied on April 17th, 2019. The soil had recently been ploughed before sampling, on March 12th. According to the farmer, the field was typically ploughed to a depth of 22-25 cm. Soil cores of a known volume were collected to a depth of 30 cm using an AMS Gator Core (American Falls, ID, USA), with five cores taken randomly along the length of each plot composited to form one representative sample per plot. Soil samples were dried at 40°C and weighed to determine bulk density based on the known volume of the soil core. After sieving to 2 mm, subsamples were taken for chemical analyses. Soil pH_{H2O} was measured in a 1:2.5 soil-to-water ratio.

2.4 Bulk Elemental Analysis

Bulk elemental composition of the GRF and soil (Dietzen et al., 2026) was determined using an iCAP™ PRO (Thermo Scientific) inductively coupled plasma optical emission spectroscopy (ICP-OES) system following lithium metaborate fusion (Carignan et al., 2001) at the Centre de Recherches Pétrographiques et Géochimiques (CRPG), CNRS, Nancy, France. These elemental data were used to estimate dissolution fractions within the SOMBA framework (Reershemius et al., 2023; Suhrhoff et al., 2025). Exchangeable cations were not extracted in advance of analysis.

Loss on ignition (LOI) of soil and GRF was determined on separate subsamples by heating the material to 1000 °C for 5 hours in order to quantify mass loss due to the combustion of organic matter and the release of remaining bound water and other volatile components that were not removed during prior drying. Elemental concentrations were subsequently normalized to a volatile-free basis prior to use in mass balance calculations by correcting for LOI, such that concentrations represent the composition of the residual mineral fraction only. This correction ensures that comparisons between treated and control soils are not biased by differences in moisture content or organic matter, which would otherwise dilute elemental concentrations on a bulk mass basis. Bulk density values used in the SOMBA framework were likewise adjusted to a volatile-free basis to ensure consistency between mass-based elemental concentrations and soil mass calculations. Inferred application rates were subsequently converted back to an initial mass basis including volatile components to correspond to the material as weighed and applied in the field.

The corrected elemental composition and maximum theoretical CO_2 uptake (CO_{2Max}) of GRF are presented in Table 1. CO_{2Max} represents the maximum theoretical CO_2 sequestration potential (kg CO_2 t^{-1} rock) assuming stoichiometric conversion of carbonic acid to bicarbonate for all released base cations (Mg^{2+}, Ca^{2+}, K^+, and $Na^{+)}$. Unlike most ERW studies, CO_{2Max} values were not adjusted using an ocean equilibration correction factor (Renforth and Henderson, 2017). Instead, carbonate speciation effects were accounted for explicitly during inorganic CO_2 uptake calculations, as described below.

Because the GRF contains a minor NaCl component, sodium concentrations were corrected to exclude the fraction associated with NaCl prior to calculation of CO_{2Max} uptake and dissolution fractions. Chlorine concentrations were used to estimate Na present as NaCl, assuming all Cl occurs as NaCl, and this Na fraction was subtracted from total Na. Only silicate-bound Na was included in subsequent SOMBA mass balance calculations.

Table 1. Average composition of glacial rock flour from the Ilulialik locality in Greenland. Reported concentrations are mean ± standard deviation (n = 9), normalized to 100% after correction for loss on ignition. Na_2O values were corrected to exclude the fraction of Na associated with the minor NaCl component of the material. CO_{2Max} represents the maximum theoretical CO_2 sequestration potential (kg CO_2 per t rock) assuming stoichiometric conversion of carbonic acid to bicarbonate for all released base cations (Mg^{2+}, Ca^{2+}, K^+, and Na^+). Non-corrected values are available in Dietzen et al. (2026).

SiO_2	Al_2O_3	Fe_2O_3	MnO	MgO	CaO	Na_2O	K_2O	P_2O_5	TiO_2	CO_{2Max}
56.1% ± 0.3	16.8% ± 0.1	8.81% ± 0.06	0.12% ± 0.001	5.07% ± 0.05	3.85% ± 0.03	3.38% ± 0.02	3.56% ± 0.04	0.75% ± 0.01	0.13% ± 0.004	252 **kg t^{-1}** ± 1.6

2.5 Soil Carbon Fractionation and Analysis

Particulate organic matter (POM) and mineral-associated organic matter (MAOM) fractions were separated based on particle size using a wet-sieving procedure following chemical dispersion, adapted from established protocols (Cambardella and Elliott, 1992; Lopez-Sangil and Rovira, 2013; Sanderman et al., 2013; Yu, 2022). Briefly, 10 g of dry, homogenized soil was dispersed in 50 ml of 0.5% sodium hexametaphosphate and mixed on a vertical rotating mixer for 18 h to disrupt macro- and

microaggregates. Immediately prior to wet sieving, samples were sonicated for 15 min and then wet-sieved over a 53 µm mesh using Milli-Q water to separate the coarse POM fraction (>53 µm) from the fine MAOM fraction (<53 µm). To ensure complete recovery of the MAOM fraction, the rinsing solution was retained and included in the MAOM fraction after evaporation of the excess water.

To ensure complete dispersion and separation of mineral material, particularly GRF associated with coarse organic matter, the retained POM fraction was re-dispersed in 10 ml of 0.5% sodium hexametaphosphate, sonicated for 5 min, mixed for an additional 30 min, and sonicated again for 10 min prior to a second wet-sieving step over a 53 µm mesh. Material passing through the sieve during this re-fractionation was combined with the MAOM fraction from the initial separation, while material remaining on the sieve was classified as POM. Final fractions were dried at 60 °C and weighed for mass balance calculations. The MAOM mass was corrected for the sodium hexametaphosphate added during dispersion.

Organic carbon concentrations were determined for both bulk soil samples and the separated POM and MAOM fractions. Bulk soil subsamples were ball-milled prior to analysis, whereas POM and MAOM samples were ground manually in an agate mortar. 250 mg of each sample was decarbonized with 10% HCl to remove inorganic carbon, after which they were dried at 105 °C for 3 h to remove residual acid. Carbon concentrations were measured in triplicate using a Multi N/C 3100 - HT 1300 TOC/TNb analyzer (Analytik Jena, Germany), with combustion at 1300 °C under an O_2 carrier gas flow of 2.2 L min^{-1} and detection by non-dispersive infrared (NDIR) spectroscopy. Based on repeated measurements of a certified reference material (NCS ZC71016; 22.3 g kg^{-1}; n = 6), the relative standard deviation was 6.9%. Soil organic carbon (SOC) stocks (t C ha^{-1}) were calculated on a fixed-depth basis (0-30 cm) using plot-specific bulk density measurements and the mean of triplicate SOC concentrations. Because plot-specific SOC stocks were not measured prior to GRF application, treatment effects were evaluated based on differences in SOC stocks between treatment and control plots at the final sampling rather than changes in SOC stocks within individual plots over time.

2.6 Statistical analysis

Categorical differences in measured parameters (soil pH_{H2O}, bulk density, bulk and fractionated SOC concentrations and stocks, and bulk soil Ti, Mg, Ca, K, and Na concentrations) were assessed using linear mixed-effects models implemented in the 'nlme' package (Pinheiro et al., 2017) in R (R Core Team, 2023), all of which included treatment (GRF or control) as a fixed effect and block as a random effect. Residual plots were inspected to ensure the assumption of normality of residuals was met. Model-based summaries were obtained using estimated marginal means implemented in the 'emmeans' package in R (Lenth, 2022). The analysis of bulk soil elemental concentrations provided both formal hypothesis tests and the treatment- and control-level means, variance components, block-level random effects, and residual distributions used as inputs for the SOMBA calculations and uncertainty propagation. Results are presented as estimated marginal means ± standard error (SE).

2.7 Assessment of Signal Resolvability

To assess signal resolvability, two distinct classes of linear mixed-effects models were employed. First, the previously described treated-control contrasts were used to evaluate whether the increase in bulk soil Ti due to feedstock application was statistically detectable despite background variability, which can be a challenge for SOMBA frameworks (Rogers and Maher, 2026). Demonstrating a resolvable immobile tracer signal is a prerequisite for application of the SOMBA framework, because this is used to infer the amount of applied material present in the sampled soil volume.

Because progressive dissolution causes concentrations of mobile cations in treated plots to converge toward control concentrations over time (Reershemius et al., 2023; Suhrhoff et al., 2025), treated-control contrasts of mobile elements are

not appropriate for assessing weathering progression. Instead, for each cation, we used the SOMBA framework to reconstruct a block-specific baseline value for comparison with the observed concentrations in the treated plots. These values represented the expected cation concentrations if the amount of GRF inferred from the observed Ti increase were added to the corresponding control plot, without any loss due to weathering. A second set of linear mixed-effects models was then fitted for each cation using a new dataset comprising the observed concentrations in the treated plots and the corresponding SOMBA-derived baseline concentrations, with data type (observed versus predicted) included as a fixed effect and block as a random effect. A statistically significant deficit relative to this reconstructed baseline was interpreted as evidence of detectable cation loss due to weathering. Cations that did not exhibit such a deficit were not considered to provide a reliable constraint on weathering.

2.8 Calculation of Dissolution Fractions

The fraction of GRF which was dissolved (τ) was quantified using a modified version of the SOMBA framework described by Suhrhoff et al. (2025), in which weathering is estimated by first inferring the contribution of applied feedstock to the soil from the concentration of an immobile tracer, such as Ti, measured in baseline soil, feedstock material, and treated post-weathering soils (Reershemius et al., 2023; Suhrhoff et al., 2025). As such, this approach also allows to infer the post-deployment but pre-weathering composition of the GRF and soil mix for treatment sites. We modified this approach by using concentrations measured in control and treated plots sampled contemporaneously as opposed to relying on paired before-and-after measurements from the same location. This change accounts for background processes that affected the entire field during the experimental period, such as the application of manure fertilizers to the entire field or seasonal biogeochemical cycling. Consequently, differences between control and treated plots can be directly attributed to the application and weathering of GRF, avoiding confounding effects that may arise when comparing samples collected several years apart from the same plot.

The increase in soil Ti concentrations was used to infer the amount of feedstock applied to the soil, which was subsequently used to reconstruct the expected concentration of mobile base cations in the soil before weathering. In this reconstruction, the cation concentrations measured in contemporaneously sampled control plots provide an estimate of the background soil composition at the time of sampling, which is assumed to represent the baseline composition in the absence of feedstock addition. The contribution of feedstock-derived cations inferred from the immobile tracer signal is then added to this baseline to estimate pre-weathering cation concentrations in treated plots for each block individually. Deviations between these reconstructed pre-weathering concentrations and the observed cation concentrations at the time of sampling are attributed to weathering losses, enabling estimation of the dissolution fraction.

Furthermore, in contrast to previously published applications of SOMBA (Reershemius et al., 2023), we did not leach cations off the exchangeable sites but instead analyzed bulk soil samples. Hence, cations that were released during GRF weathering but are still stored on exchangeable sites or in secondary phases are still present in the samples. This has the benefit that τ is a more direct measure of realized CDR, reflecting cations that have been both released from the feedstock and transported out of the plough layer, without the need to account for CDR losses due to exchangeable processes or secondary phase formation within the system boundary.

The dissolution fraction (τ) and corresponding GRF application amount were calculated for each cation individually by inserting mean control and treated concentrations together with the site-average soil bulk density (also used to represent feedstock bulk density) into the SOMBA equations.

2.9 Uncertainty Propagation

Reported uncertainty was quantified using a parametric hierarchical bootstrap tailored to the randomized block design (Dietzen et al., 2026). Given the small number of blocks (n = 4), model-based resampling was used to obtain stable variance estimates. This approach will likely always be necessary in similar experimental field trials, as the number of replicate blocks is unlikely to be high enough for non-parametric bootstrapping. Previously described linear mixed-effects models fitted to Ti and each mobile cation provided estimates of fixed effects, block-level random effects, and residual variability. For each of 3,000 bootstrap replicates, block-level random effects and residuals were resampled from the fitted mixed models and combined with the estimated fixed effects to generate synthetic control and treated observations. Within each bootstrap iteration, reconstructed concentrations were averaged across resampled blocks to obtain mean inputs for the SOMBA calculations. Bulk density was propagated analogously by resampling block-level bulk densities (mean of all plots within a block), with feedstock bulk density assumed equal to this value. Analytical uncertainty in feedstock composition was incorporated by sampling tracer concentrations from normal distributions defined by measured means and standard deviations (Table 1). The SOMBA equations were applied to each replicate to generate distributions of τ and application rate, which were summarized using the standard deviation (SD) and 95% confidence intervals (CI).

2.10 Determining inorganic CO_2 uptake

In ERW studies, inorganic CO_2 uptake is commonly estimated either from bicarbonate generation and export from the soil system or from exported charge-balance alkalinity converted to long-term atmospheric CO_2 removal using established equilibration factors based on ocean carbonate speciation. As alkalinity is transported through soils, groundwater, and river systems toward the ocean, carbonate equilibria continuously adjust in response to changing pH and partial pressure of CO_2 (pCO_2) conditions (Bertagni and Porporato, 2022; Zhang et al., 2025). Because the ocean is substantially more alkaline than the soil solution of most agricultural soils used for ERW, owing to both inherent soil acidity and elevated soil pCO_2 (Dietzen and Rosing, 2023), the effective carbon-capture efficiency is likely to increase during downstream transport. This efficiency ultimately approaches the ocean-buffered conversion factor used in most ERW studies, which typically apply ocean correction factors of ranging from 80-90% (Bertagni and Porporato, 2022; Kanzaki et al., 2023; Renforth and Henderson, 2017). However, when carbonate speciation under soil conditions is also accounted for explicitly, sequential application of both soil- and ocean-based correction factors may inadvertently over-correct carbon-capture efficiency, as these corrections are not additive. Here, initial inorganic CO_2 uptake is quantified at the point of alkalinity generation in the soil solution where GRF dissolution occurs, while longer-term atmospheric removal after downstream transport and equilibration with ocean carbonate chemistry is considered separately.

In Dietzen & Rosing (2023), we introduced a framework to estimate the fraction of mineral-derived base cations balanced by bicarbonate generation under soil conditions. Mineral dissolution in soils is driven by multiple proton sources, including carbonic acid as well as other inorganic and organic acids (Holden et al., 2024). These acids contribute to the total proton supply for weathering and influence carbonate speciation in the soil solution. Consequently, only a fraction of mineral-derived base cations is balanced by bicarbonate formation, meaning that the carbon-capture efficiency of weathering depends on the chemical conditions of the soil solution. The correction framework is based on carbonate system equilibria and uses soil pH and pCO_2 to estimate the fraction of mineral dissolution that generates bicarbonate and carbonate (carbonate alkalinity), conceptually similar to the alkalinization carbon-capture efficiency (ACE) factor defined by Bertagni and Porporato (2022), and here referred to as the carbonate alkalinity conversion factor.

In our previous application of this framework, laboratory-measured soil pH values were used directly to calculate the carbonate alkalinity conversion factor (Dietzen and Rosing, 2023). However, these measurements are determined under

equilibrium with atmospheric pCO_2 (~400 ppm) and therefore do not represent *in situ* soil conditions, where pCO_2 is typically elevated (Elberling and Matthiesen, 2007; Matthiesen, 2004). Because carbonate speciation depends on both pH and pCO_2, failure to account for elevated soil pCO_2 and its impacts on *in situ* pH can bias estimates of bicarbonate generation efficiency. This bias causes the fraction of dissolution that generates bicarbonate to be overestimated when laboratory-measured soil pH (pH_{H2O}) exceeds approximately 5.6 and underestimated when it falls below this value.

In the updated framework, laboratory-measured pH_{H2O} values, determined under equilibrium with atmospheric pCO_2, are first used to infer the corresponding alkalinity of the soil solution. Assuming this alkalinity is conserved, carbonate equilibria are then solved for the selected *in situ* soil pCO_2, yielding the corresponding *in situ* pH values and the carbonate speciation of the soil solution. These adjusted pH values are then used, together with the corresponding pCO_2, to estimate the carbonate alkalinity conversion factor (see Dietzen et al., 2026 for calculator). When selecting the input pH_{H2O} values, it is important to account for both differences between treated and control soils and temporal variation in soil pH. To address this variability, we employed a site-specific range of pH_{H2O} values in combination with a broad range of pCO_2 values (1,000–40,000 ppm) to define upper and lower bounds for the carbonate alkalinity conversion factor at this site. Because direct measurements of soil pCO_2 were not available and soil pCO_2 varies spatially and temporally, this range-based approach was used to bound uncertainty in the conversion factor. The resulting predicted *in situ* pH values were then used, together with the corresponding input soil pCO_2 values, to calculate a range of carbonate alkalinity conversion factors.

The bicarbonate generation estimated through this framework using soil pH and pCO_2 as inputs represents the initial CO_2 uptake associated with ERW under the carbonate chemistry conditions of the soil solution prior to transport of weathering products. However, on longer-term timescales the atmospheric impact will depend on the net charge-balance alkalinity exported from the terrestrial system and the carbonate speciation conditions under which that alkalinity ultimately equilibrates, primarily in the ocean (Kanzaki et al., 2023; Renforth and Henderson, 2017). The timescale over which this equilibration occurs is both uncertain and highly variable across systems, such that the appropriate conversion factor and associated crediting timescale must be evaluated on a case-by-case basis.

Accordingly, we report inorganic CO_2 uptake as a range bounded by (i) the initial bicarbonate generation estimated from carbonate equilibria under soil solution conditions and (ii) long-term atmospheric removal after equilibration with ocean carbonate chemistry. These estimates do not deduct cations temporarily taken up by plants, under the simplifying assumption that upon decomposition of the organic matter that these cations are bound in, the charge-balance alkalinity will be regenerated (Bijma et al., 2026). Potential losses or transformations of alkalinity due to secondary mineral precipitation in deeper soils or streams are also not accounted for (Clarkson et al., 2024), and the timescale over which full equilibration with ocean conditions occurs remains uncertain and is not explicitly modeled.

3. Results

3.1 Signal resolvability

A significant increase of 104 ± 17 ppm in Ti concentration was observed in treated soils relative to controls ($p = 0.009$), confirming that the applied feedstock signal was statistically resolvable against background variability (Table 2).

Table 2. **Estimated marginal means ± standard error (SE) and contrasts from mixed-effects models comparing treated (T) vs. control (C) concentrations (ppm) at the time of sampling (approximately 5 years after treatment) for Ti and mobile cations. Differences (Δ) and *p* values are based on linear mixed-effects model contrasts.**

Element	Control ± SE	Treated ± SE	Δ (T − C) ± SE	*p* value
Ti	1,405 ± 19	1,509 ± 18	104 ± 17	0.009
Mg	639 ± 34	987 ± 34	349 ± 45	-
Ca	3,795 ± 103	3,994 ± 103	200 ± 119	-
K	11,191 ± 196	11,258 ± 196	67 ± 277	-
Na	5,483 ± 159	5,615 ± 159	132 ± 184	-

Observed treated concentrations of Mg were significantly lower than their predicted post-application concentrations under the assumption of no loss ($p = 0.013$), indicating detectable cation depletion consistent with weathering (Table 3). Differences between predicted and observed concentrations for Ca, K, and Na were not statistically significant.

Table 3. **Estimated marginal means ± standard error (SE) and contrasts from mixed-effects models comparing predicted post-application (P) vs observed treated (T) concentrations (ppm) for mobile cations. Differences (Δ) and *p* values are based on linear mixed-effects model contrasts.**

Element	Predicted ± SE	Treated ± SE	Δ (P − T) ± SE	*p* value
Mg	1,436 ± 95	987 ± 95	449 ± 85	0.013
Ca	4,402 ± 136	3,994 ± 136	407 ± 145	0.068
K	11,651 ± 195	11,258 ± 195	393 ± 151	0.080
Na	5,992 ± 184	5,615 ± 184	377 ± 121	0.052

3.2 Dissolution fraction, weathering rate, and inferred GRF application rate

Magnesium yielded a dissolution fraction (τ) of 0.56 (SD: 0.06; 95% CI: 0.43-0.66), representing the most tightly constrained estimate among the measured cations (Table 4, Fig. 1). Sodium yielded a mean τ of 0.73 (SD: 0.26; 95% CI: 0.25-1.21), calcium yielded a mean τ of 0.67 (SD: 0.14; 95% CI: 0.42-0.99), and potassium yielded a mean τ of 0.85 (SD: 0.55; 95% CI: 0.06-2.20). Although the central estimates for Ca, Na, and K were comparable to or greater than the Mg-derived value, their uncertainty intervals were substantially wider, consistent with the fact that the differences between predicted post-application concentrations and observed treated concentrations were not statistically significant.

Table 4. **Cation-specific dissolution fraction (τ) and corresponding estimated one-time application rate calculated directly from measured elemental concentrations. Standard deviations (SD) and 95% confidence intervals (CI) were derived from parametric hierarchical bootstrap resampling to quantify uncertainty in the estimates.**

Cation	τ ± SD	95% CI	Application Rate (t ha^{-1}) ± SD	95% CI
Mg	0.56 ± 0.06	0.43-0.66	44.6 ± 4.8	35.9-54.3
Ca	0.67 ± 0.14	0.42-0.99	42.9 ± 5.2	33.1-53.2
K	0.85 ± 0.55	0.06-2.20	40.5 ± 8.2	25.7-57.5
Na	0.73 ± 0.26	0.25-1.21	42.1 ± 6.0	31.3-54.6

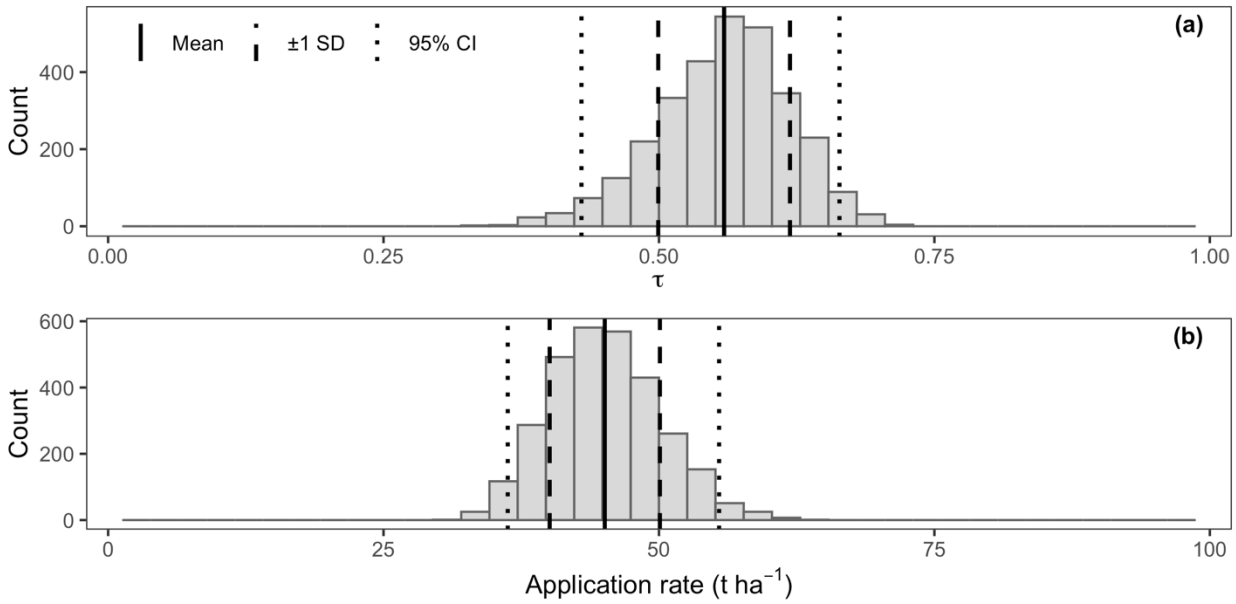


Figure 1. **Bootstrap distributions of the dissolution fraction (τ) (a) and inferred one-time GRF application rate (b) based on Mg and the immobile tracer Ti. Histograms show results from 3,000 hierarchical bootstrap realizations that propagate block-level variability, residual error, and feedstock compositional uncertainty. Solid lines indicate the mean of the bootstrap distribution, dashed lines represent ±1 standard deviation, and dotted lines denote the 95% confidence interval bounds.**

When expressed as the total positive charge released, calculated by summing the contributions of each cation based on its weathering fraction and normalizing by the total positive charge contained in the applied GRF, approximately 66% of the base-cation charge potential was mobilized over the five-year period. However, because Mg provided the only statistically resolvable signal and the narrowest uncertainty bounds, the Mg-derived dissolution fraction of 56.3% is considered the most robust and conservative single-cation constraint on overall feedstock weathering. This value is therefore used to calculate the surface-area-normalized weathering rate and to estimate CO_2 uptake. Based on this Mg-derived dissolution fraction and the BET surface area of the material as measured in Sarkar (2021), the corresponding surface-area-normalized weathering rate (Wr) over the five-year period is 1.06×10^{-12} mol m^{-2} s^{-1} (log Wr = −11.97).

3.3 GRF Application Rate

There was no significant difference in bulk density between the control and treated plots (Table 5). Having been sampled shortly after tillage, soil bulk density was unusually low, averaging 0.61 g cm^{-3} across the site and indicating that the 0-30 cm sampling depth corresponded to a shallower equivalent mass depth than intended. Using bulk density measurements from the subsequent year (1.07 g cm^{-3}), obtained under more representative conditions, the sampled interval was estimated on an equivalent soil mass basis to correspond to approximately the upper 17 cm of the soil profile. The reported plough depth at the site was approximately 22 to 25 cm. If 50 t ha^{-1} of GRF were uniformly mixed throughout the plough layer,

approximately 23 to 32% of the applied material would be expected below the sampled interval at the time of sampling. Under this assumption, the effective application amount within the sampled layer would range from approximately 34 to 38.5 t ha^{-1}.

The Mg-based application amount inferred through the SOMBA framework was 44.6 t ha^{-1}, with a bootstrap-derived standard deviation of 4.8 t ha^{-1} and a 95% confidence interval of 35.9-54.3 t ha^{-1} (Table 4). Though considered less reliable indicators, inferred application rates based on Ca, K, and Na were comparable (42.9, 40.5, and 42.1 t ha^{-1}, respectively).

Table 5. Estimated marginal means (± SE) of soil properties [pH_{H2O}, bulk density, mass fraction of particulate organic matter (POM), and mineral-associated organic matter (MAOM), and C concentrations of POM, MAOM, and bulk soil (SOC), and corresponding C stocks (t ha^{-1}] for control (C) and GRF-treated (T) plots. Carbon concentrations (% C) for POM and MAOM refer to the C concentration within the respective isolated fraction, whereas SOC (% C) refers to the C concentration of bulk soil. Differences (Δ) and *p* values are based on linear mixed-effects model contrasts.

	Control ± SE	Treated ± SE	Δ (T − C) ± SE	*p* value
pH_{H2O}	5.92 ± 0.05	5.93 ± 0.05	0.01 ± 0.07	0.884
Bulk Density (g cm^{-3})	0.60 ± 0.04	0.61 ± 0.04	0.01 ± 0.03	0.674
POM (fraction)	0.85 ± 0.01	0.83 ± 0.01	−0.01 ± 0.01	0.084
MAOM (fraction)	0.16 ± 0.01	0.17 ± 0.01	0.01 ± 0.01	0.084
POM (% C)	0.25 ± 0.02	0.29 ± 0.02	0.04 ± 0.03	0.232
MAOM (% C)	13.9 ± 0.2	13.6 ± 0.2	−0.3 ± 0.2	0.271
SOC (% C)	2.52 ± 0.11	2.76 ± 0.11	0.24 ± 0.14	0.172
POM C (t ha^{-1})	3.87 ± 0.32	4.37 ± 0.32	0.50 ± 0.35	0.249
MAOM C (t ha^{-1})	38.7 ± 2.5	41.6 ± 2.5	2.9 ± 1.5	0.156
SOC C (t ha^{-1})	45.3 ± 2.3	50.3 ± 2.3	5.0 ± 0.5	0.002

3.4 CO_2 Sequestration Estimate

Initial CO_2 uptake via ERW was estimated after accounting for the impact of soil pH on carbonate speciation. Mean soil pH_{H2O} at the five-year sampling point was 5.94, with no statistically significant difference between treatment and control (Table 5). Likewise, there was no significant difference in pH with treatment after the first growing season, when mean soil pH_{H2O} was 5.79 (Dietzen and Rosing, 2023).

Laboratory-measured pH values from both time points were recalculated to reflect equilibrium with a plausible range of soil pCO_2 (1,000-40,000 ppm). Under these conditions, estimated in situ soil pH ranged from 4.60 to 5.62. Under these in situ pH and pCO_2 conditions, the carbonate alkalinity conversion factor was estimated to range from 0.45 to 0.69 (Fig. 2), corresponding to a soil-solution CO_2 uptake of 3.2-4.9 t CO_2 ha^{-1}. Accounting for ocean carbonate equilibration, whereby the carbonate alkalinity conversion factor evolves toward 0.8-0.9 (Bertagni and Porporato, 2022; Kanzaki et al., 2023; Renforth and Henderson, 2017), the corresponding long-term atmospheric CO_2 reduction is estimated at 5.7-6.4 t CO_2 ha^{-1}, assuming that all alkalinity generated by GRF weathering is ultimately exported to the ocean, without substantial attenuation or reversal during terrestrial and downstream transport.

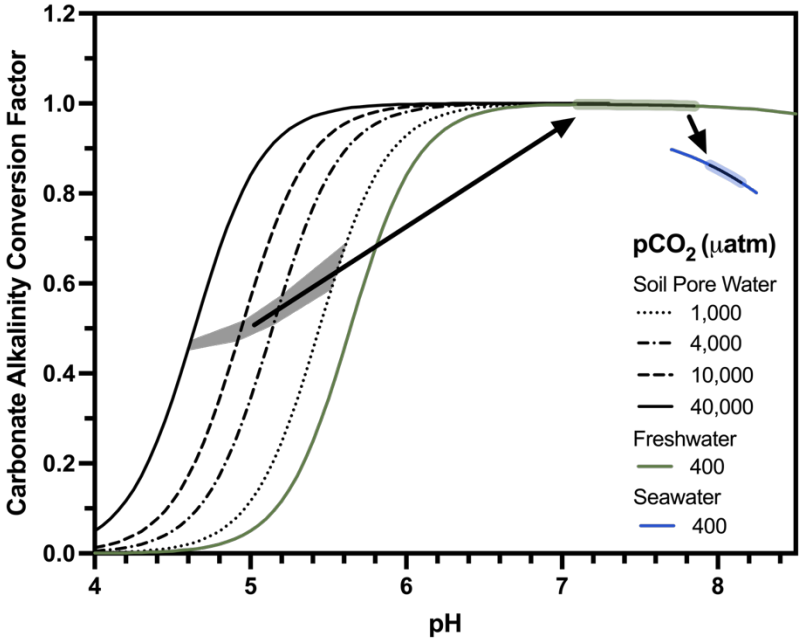


Figure 2. Carbonate alkalinity conversion factor as a function of pH and pCO_2 across representative soil (Dietzen and Rosing, 2023), surface freshwater, and ocean conditions (Bertagni and Porporato, 2022; Kanzaki et al., 2023; Renforth and Henderson, 2017)**.** The figure illustrates how the carbonate alkalinity conversion factor associated with cations released during ERW at Vojens could change as alkalinity is transported from acidic, high-pCO_2 soil pore waters through surface freshwater and ultimately to coastal seawater. The shaded areas represent the range of conversion factors represented by these conditions, with arrows indicating the potential evolution from local soil conditions, through surface freshwater represented by local Danish streams (Danmarks Miljøportal, 2026), to coastal seawater in the Lillebælt (Carstensen et al., 2021). For acidic conditions (pH < 7), conversion factors were calculated following Dietzen and Rosing (2023); for basic conditions (pH > 7), conversion factors for freshwater and seawater were calculated following Bertagni and Porporato (2022). All curves are calculated for water at 15 °C; the conversion factor varies with temperature, particularly in seawater. At higher pH, the conversion factor generally declines as carbonate speciation shifts from HCO_3^- toward CO_3^{2-}, while the different behavior of freshwater and seawater reflects the influence of salinity on carbonate speciation.

3.5 Soil Organic Carbon

No statistically significant differences were detected in carbon concentration for bulk SOC, POM, or MAOM. Carbon concentrations in treated plots were highly variable but were generally higher than the control for bulk SOC and the POM fraction, whereas MAOM carbon concentrations were lower, consistent with dilution of the fine fraction resulting from the addition of GRF. MAOM comprised 91% of total SOC on average.

In contrast, total SOC stocks were significantly higher in GRF-treated plots compared to controls ($p = 0.002$). Given that bulk density did not differ significantly between treatments, the observed difference in SOC stocks was not attributable to treatment effects on soil mass. Mean SOC stocks were higher in treated plots (50.3 t C ha^{-1}) than in control plots (45.3 t C ha^{-1}), corresponding to a treatment difference of 5.0 t C ha^{-1} (equivalent in carbon mass to 18.3 t CO_2 ha^{-1}). When expressed as areal carbon stocks, both MAOM and POM exhibited non-significant increases (2.89 t C ha^{-1} and 0.5 t C ha^{-1}, respectively).

4. Discussion

4.1 Substantial weathering under temperate field conditions

This five-year field assessment demonstrates substantial dissolution of GRF in temperate agricultural soils, with at least 56 ± 6% of the applied material weathered over this period. The corresponding surface-area-normalized rate of total alkalinity release (1.06×10^{-12} mol TA m^{-2} s^{-1}; log Wr = −11.97) indicates that rapid silicate weathering can occur in temperate

croplands despite lower temperatures and precipitation than tropical regions, where weathering is expected to be fastest (Edwards et al., 2017). This rate is comparable to those reported in soil incubation and short-term mesocosm experiments for basaltic feedstocks, which typically report surface-area-normalized weathering rates between log Wr = −11 and −12 mol m^{-2} s^{-1} (Kelland et al., 2020; te Pas et al., 2023; Reershemius et al., 2023; Vienne et al., 2024). Likewise, dissolution fractions reported in multi-year agricultural trials of basalt in the U.S. Midwest are broadly comparable to those observed here, despite differences in feedstock, application frequency, and soil type (Beerling et al., 2024; Kantola et al., 2023). These similarities are somewhat surprising as they suggest that despite being derived from granitic bedrock, which is expected to be less chemically reactive than basaltic rocks, GRF exhibits comparable rates of surface area normalized alkalinity release. Combined with the exceedingly fine surface area, this may imply that the overall alkalinity release from GRF may proceed more quickly than from coarser basaltic feedstocks.

4.2 Implications for MRV

The substantially higher dissolution fraction inferred using SOMBA relative to earlier exchangeable-cation-based estimates indicates that point measurements may substantially underestimate cumulative weathering. Previously, weathering at this site was estimated at 7.9% over approximately 2.5 years based on repeated measurements of soil exchangeable Mg (Dietzen and Rosing, 2023). In contrast, application of the SOMBA framework yields a dissolution fraction of 56.3% of Mg over five years. Because silicate weathering rates are generally expected to decline over time as reactive surface area decreases (Brantley, 2025; Power et al., 2025), it is unlikely that accelerated dissolution in later years explains this discrepancy. Rather, the difference suggests that exchangeable Mg measurements did not capture Mg released and subsequently leached during high-precipitation periods. Sampling during the growing season captured transient Mg accumulation under limited leaching but failed to quantify winter losses, leading to substantial underestimation of cumulative dissolution. These results highlight the importance of time-integrated approaches for MRV, as point measurements of exchangeable cations or pore water may not capture the full flux of weathering products exported from the soil system.

Not all cations provided equally robust constraints on dissolution. Here, a cation provides a robust constraint when its depletion relative to the predicted no-weathering concentration can be resolved against background soil variability. Only Mg showed statistically significant differences between predicted and observed treated concentrations, whereas Ca, Na, and K exhibited wider uncertainty intervals due to larger and more heterogeneous background soil pools (Suhrhoff et al., 2024). Background concentrations of Ca and Na were approximately one order of magnitude greater than those of Mg, while K concentrations were roughly two orders of magnitude greater than Mg, with correspondingly higher spatial variability. This elevated background variability reduced sensitivity to treatment-induced changes. Consequently, the Mg-based weathering fraction represents the most defensible single-element estimate and can be considered conservative, as dissolution fractions inferred for other cations were consistently higher. Despite these differences in precision, dissolution fractions were broadly consistent across base cations, supporting the overall magnitude of weathering inferred from SOMBA.

These results highlight that background soil variability imposes a fundamental constraint on the detectability of weathering signals in field settings (Rogers and Maher, 2026; Suhrhoff et al., 2024) but also demonstrate that this limitation can be mitigated through careful experimental design. Application rates derived from SOMBA were consistent with the estimated mass of GRF present within the sampled soil layer, with the 95% confidence intervals of the inferred rates overlapping this estimate across all elements. This agreement reflects favorable experimental conditions, including repeated ploughing that promoted thorough mixing of the feedstock within the plough layer and a randomized block design that accounted for within-field heterogeneity, a key challenge for soil mass balance approaches (Rogers and Maher, 2026). Together, these factors enabled a sufficiently clear geochemical signal to constrain dissolution despite large background pools.

In less controlled settings, incomplete mixing and greater spatial heterogeneity are likely to obscure treatment signals and increase uncertainty in SOMBA-derived estimates. These challenges may be particularly pronounced in shorter-duration studies with incomplete mixing via repeated tillage or when experimental designs do not explicitly account for background variability. While randomized block designs may be impractical for commercial deployments, experimental field trials aimed at evaluating ERW should incorporate these principles wherever possible. In commercial applications, although there may be incentives to quantify weathering rapidly for crediting purposes, allowing more time for tillage to homogenize the amendment within the plough layer may ultimately produce clearer geochemical signals and reduce the analytical effort required to detect weathering.

The substantially higher dissolution fraction inferred from SOMBA also implies a major upward revision of estimated CO_2 uptake relative to the previously reported estimate of 728 kg CO2 ha^{-1} in Dietzen & Rosing (2023). In the present analysis, cumulative dissolution is estimated at approximately 56% after five years, corresponding to initial CO_2 uptake of 3.2–4.9 t CO_2 ha^{-1}, depending on carbonate speciation in the soil solution. Even at the lower bound, this represents an approximately fivefold increase relative to the previous estimate. This estimate represents CO_2 uptake associated with weathering within the soil system and does not by itself establish the magnitude or timescale of permanent atmospheric CO_2 removal. The latter depends on the subsequent transport and fate of the generated alkalinity beyond the soil profile, including its eventual equilibration with ocean carbonate chemistry (see Section 4.4).

4.3 Organic Carbon Dynamics

In addition to inorganic carbon removal, GRF application was associated with a significant difference in SOC stocks of 5.0 t C ha^{-1} between treatment and control plots, equivalent to the storage of an additional 18.3 t CO_2 ha^{-1} in soil carbon pools (Table 5). In contrast, SOC concentrations did not differ significantly between treatments, and bulk density was likewise not significantly affected when analyzed independently. Because SOC stocks integrate both carbon concentration and bulk density, which are often inversely related (Harbo et al., 2022; Sakin, 2012), expressing SOC on an area basis reduced residual variance and revealed a consistent treatment effect on carbon stocks.

Notably, this organic carbon increase exceeds the maximum theoretical CO_2 uptake achievable through full dissolution of the GRF and is more than double the CO_2 uptake inferred from the observed dissolution fraction. These findings indicate that organic carbon dynamics may represent a substantial component of the total climate impact of GRF application. This observation is consistent with growing evidence that organic carbon responses can represent a major component of the climate benefit associated with ERW, in some cases exceeding inorganic carbon sequestration through alkalinity generation (Anthony et al., 2025; Vicca et al., 2022; Xu et al., 2024).

Reported responses of SOC to mineral amendments vary widely across studies, reflecting strong context dependency related to soil properties, climate, plant communities, and experimental duration. Several studies report initial losses of soil organic matter following mineral additions, often attributed to stimulated microbial activity and accelerated decomposition of existing mineral-associated organic matter pools (Boito et al., 2025; Fang et al., 2023; Niron et al., 2024; Sokol et al., 2024). However, longer-term observations (Sohng et al., 2025; Sokol et al., 2024; Steinwidder et al., 2025) and meta-analyses of the effects of liming (Wang et al., 2021; Zhang et al., 2022) suggest that these early losses may represent transient responses, with systems transitioning toward net SOC accumulation after one to several years as stabilization processes and increased carbon inputs begin to dominate. Similar temporal dynamics have been reported following agricultural liming, where increased microbial activity can initially stimulate organic matter mineralization but longer-term improvements in soil fertility and plant productivity increase carbon inputs and ultimately promote SOC accumulation (Paradelo et al., 2015). Our

five-year observations are consistent with this longer-term phase in which stabilization processes outweigh early-stage decomposition.

Although increases in POM and MAOM carbon stocks were not statistically significant when considered individually, reflecting the greater variability in the fractionation data, the magnitude of the observed difference was substantially larger for MAOM (+2.89 t C ha^{-1}) than for POM (+0.50 t C ha^{-1}). Given that MAOM comprises over 90% of SOC at this site, the relatively large observed difference in MAOM carbon stocks is consistent with a potential contribution of mineral-associated stabilization to the overall SOC response. Although the present data do not provide sufficient evidence to determine the underlying mechanism, this interpretation is supported by evidence from other ERW trials, in which mineral additions increase reactive surface area for organo-mineral interactions and may promote the stabilization of organic carbon (Boito et al., 2025; Niron et al., 2024; Ramos et al., 2024; Steinwidder et al., 2025; Xu et al., 2024). The effect may be particularly pronounced in coarse-textured sandy soils such as the one studied here, where mineral surface area for organic matter stabilization is initially limited. In the case of GRF, the high surface area of the applied material itself may provide abundant reactive mineral surfaces capable of facilitating MAOM formation following application.

Assessing SOC responses in this sandy context provides insight into how ERW may alter carbon stabilization pathways in soils that are initially limited in reactive mineral surfaces (Georgiou et al., 2022; Slessarev et al., 2022). These findings indicate that ERW can contribute to climate mitigation not only through inorganic carbon sequestration but also by promoting organic carbon stabilization in agricultural soils, highlighting the importance of incorporating SOC dynamics into ERW monitoring and verification frameworks. Beyond carbon sequestration, increases in SOC are associated with improved soil structure, nutrient retention, and water-holding capacity (Schjønning et al., 2018; Tiessen et al., 1994), suggesting potential co-benefits for agricultural sustainability.

4.4 Potential for GRF Application in Denmark

Extrapolating the results of the present field trial to the broader Danish agricultural context suggests a substantial theoretical CDR potential for ERW on sandy soils in Western Denmark. Denmark has approximately 2.6 million hectares of utilized agricultural area, of which an estimated 31%, roughly 807,000 ha, is classified as sandy soils broadly comparable to the Vojens field site (Statistics Denmark, 2026; Styczen and Sørensen, 2004). Applying the trial application amount of 50 t ha^{-1} across this area would correspond to a total application of approximately 40 million tons of GRF. Assuming that the weathering response and carbonate speciation observed at Vojens are representative of GRF application across this area, approximately 56% of the applied GRF could be expected to weather over five years, corresponding to an initial CO_2 uptake of approximately 2.6–4.0 million tons of CO_2 over the same period. The corresponding ocean-equilibrated CDR potential would be greater (4.6-5.2 million tons of CO_2), but represents a conditional long-term endpoint dependent on transport of the generated alkalinity out of the terrestrial system and its eventual equilibration with ocean carbonate chemistry. This should therefore be regarded as a long-term theoretical potential rather than an expected near-term removal.

The extent to which the higher, ocean equilibrated CDR potential is realized in practice depends on the transport and long-term fate of the generated alkalinity. Related evidence from agricultural liming in the Mississippi River Basin indicates that substantial time lags can occur between mineral amendment and downstream alkalinity export. Both long-term river fluxes and reactive transport modelling independently suggested lag times on the order of decades, reflecting the retention and release of base cations within soils as well as hydrological transport (Suhrhoff et al., 2026b). The magnitude of such lags is likely to be strongly site-dependent, however, depending on factors including soil exchange capacity and acidity pools, hydrology, and amendment characteristics.

From a hydrological perspective, transport of solutes from agricultural fields towards streams and ultimately the oceans is likely relatively rapid at the Vojens field site. The sandy outwash landscapes of western Jutland, low-relief topography, highly permeable glacial sediments, and a dense surface water network result in strong groundwater-surface water connectivity (Duque et al., 2023; Klimadatastyrelsen, 2026). Such conditions would favor relatively rapid hydrological transport of dissolved weathering products from soils towards coastal waters. movement of dissolved cations and alkalinity out of the soil profile. However, rapid hydrological transport does not necessarily translate into rapid or permanent atmospheric CO_2 removal, because these conditions do not preclude geochemical attenuation of alkalinity along the transport path. Such processes can delay the export of alkalinity and, where weathering-derived cations are subsequently re-acidified within the terrestrial system, can also reverse some of the CO_2 uptake associated with their initial release from the mineral. Recent evidence suggests that a substantial fraction of the generated alkalinity may be consumed by reactions with acidic subsoils in this region before reaching the ocean, delaying permanent atmospheric CO_2 removal by decades even under these relatively favorable hydrological conditions (Jessen et al., 2026).

Overall, the Vojens results indicate substantial weathering and associated initial CO_2 uptake over five years, but the extent, permanence, and timing of atmospheric CO_2 removal cannot be inferred from soil weathering alone. Quantifying the fraction of weathering-derived alkalinity that is ultimately exported from agricultural soils, the timescale of transport, and the extent to which alkalinity and weathering-derived cations are retained or consumed along the transport pathway will require coupled hydrological and reactive transport modelling together with measurements of deeper soil profiles and groundwater. Improving our understanding of alkalinity transport and attenuation therefore represents a key research priority for robust MRV and realistic regional estimates of enhanced weathering CDR.

Conclusion

This five-year field experiment provides rare, time-integrated constraints on ERW under temperate agricultural conditions. Using a soil mass balance framework within a randomized block design, we estimate that at least 56% of the applied glacial rock flour weathered over five years, based on the proportion of its constituent cations that were lost from the topsoil. These results demonstrate that finely grained silicate materials can undergo substantial dissolution in well-drained sandy soils, highlighting the importance of hydrological flushing and reactive surface area in maintaining mineral–solution disequilibrium under field conditions.

Accounting for carbonate system constraints under realistic soil pCO_2 conditions, this degree of dissolution corresponds to an initial inorganic CO_2 uptake of 3.2–4.9 t CO_2 ha^{-1}, with a potential long-term atmospheric removal of 5.7-6.4 t CO_2 ha^{-1} assuming complete transport of the generated alkalinity to the ocean and subsequent equilibration with ocean carbonate chemistry. These estimates substantially exceed earlier site-specific assessments based on exchangeable cation measurements, indicating that point measurements can underestimate cumulative weathering and reinforcing the need for time-integrated approaches for MRV.

In parallel, SOC stocks were significantly higher in the GRF-treated plots than the control plots, with a difference of 5.0 t C ha^{-1} (18.3 t CO_2 ha^{-1}). Although the mechanisms cannot be uniquely resolved, the predominance of gains in the mineral-associated fraction is consistent with enhanced organo-mineral stabilization in this coarse-textured soil. The magnitude of this response indicates that organic carbon dynamics may represent a substantial component of the climate impact of ERW.

Together, these findings provide field-based evidence that ERW of glacial rock flour can drive substantial carbon sequestration through both inorganic and organic pathways over multi-year timescales. More broadly, the results highlight

549 the importance of combining time-integrated geochemical methods with soil carbon measurements to constrain the full
550 carbon balance of enhanced weathering systems and support the development of robust, field-deployable MRV frameworks
551 for agricultural carbon removal.

552 **Code and data availability**

553 Soil and feedstock data, R code, and the updated carbon-capture efficiency calculator can be accessed at:
554 https://doi.org/10.17894/ucph.63ae53e9-9269-4021-8f25-084dcbdf9459

555 **Author contributions**

556 Conceptualization: MTR, CD; methodology: CD, MR, TJS; formal analysis: CD; investigation: CD and MR; writing-
557 original draft: CD and MR; writing review & editing: CD, MR, TJS, and MTR; visualization: CD; supervision: MTR;
558 project administration: CD; funding acquisition, MTR.

559 **Competing interests**

560 Minik Thorleif Rosing is Chairman of the Board for the Rock Flour Company, a Danish Start-up company aiming at
561 developing glacial rock flour for climate change mitigation and global food security. Christiana Dietzen served as a scientific
562 advisor to the company until the end of 2025. Neither author received financial compensation for these roles, but Rosing has
563 invested personal equity for starting the company. The Rock Flour Company has not influenced the study and has no
564 commercial interests in the research reported here. The remaining authors have no relevant financial or non-financial
565 interests to disclose.

566 **Disclaimer**

567 Copernicus Publications remains neutral with regard to jurisdictional claims made in the text, published maps, institutional
568 affiliations, or any other geographical representation in this paper. While Copernicus Publications makes every effort to
569 include appropriate place names, the final responsibility lies with the authors. Views expressed in the text are those of the
570 authors and do not necessarily reflect the views of the publisher.

571 **Acknowledgements**

572 The authors would like to thank the Novo Nordisk Foundation for funding this research. Tim Jesper Suhrhoff acknowledges
573 funding from the Yale Center for Natural Carbon Capture. We would also like to acknowledge Lars Stoumann Jensen and
574 Klara Cecilia Gunnarsen, who designed and organized the installation of the field trial, the farmer Flemming Skov, and the
575 personnel at SEGES (National agricultural knowledge and innovation center) and SLF (Sønderjysk Landboforening), who
576 managed the site for the first three years of the experiment. Claude and ChatGPT were used to assist in converting the
577 Python implementation of the SOMBA framework published in Suhrhoff et al. (2025) into R code and in modifying the
578 framework to incorporate the use of a randomized block design.

Financial support

This work was funded by the Novo Nordisk Foundation (grant number: NNF22SA0079616).

References

Anthony, T. L., Jones, A. R., and Silver, W. L.: Supplementing Enhanced Weathering With Organic Amendments Accelerates the Net Climate Benefit of Soil Amendments in Rangeland Soils, AGU Advances, 6, e2024AV001480, https://doi.org/10.1029/2024AV001480, 2025.

Basile-Doelsch, I., Balesdent, J., and Pellerin, S.: Reviews and syntheses: The mechanisms underlying carbon storage in soil, Biogeosciences, 17, 5223–5242, https://doi.org/10.5194/bg-17-5223-2020, 2020.

Beerling, D. J., Leake, J. R., Long, S. P., Scholes, J. D., Ton, J., Nelson, P. N., Bird, M., Kantzas, E., Taylor, L. L., Sarkar, B., Kelland, M., DeLucia, E., Kantola, I., Müller, C., Rau, G., and Hansen, J.: Farming with crops and rocks to address global climate, food and soil security, Nature Plants, 4, https://doi.org/10.1038/s41477-018-0108-y, 2018.

Beerling, D. J., Epihov, D. Z., Kantola, I. B., Masters, M. D., Reershemius, T., Planavsky, N. J., Reinhard, C. T., Jordan, J. S., Thorne, S. J., Weber, J., Val Martin, M., Freckleton, R. P., Hartley, S. E., James, R. H., Pearce, C. R., DeLucia, E. H., and Banwart, S. A.: Enhanced weathering in the US Corn Belt delivers carbon removal with agronomic benefits, Proceedings of the National Academy of Sciences, 121, e2319436121, https://doi.org/10.1073/pnas.2319436121, 2024.

Beerling, D. J., Reinhard, C. T., James, R. H., Khan, A., Pidgeon, N., and Planavsky, N. J.: Challenges and opportunities in scaling enhanced weathering for carbon dioxide removal, Nat Rev Earth Environ, 6, 672–686, https://doi.org/10.1038/s43017-025-00713-7, 2025.

Bertagni, M. B. and Porporato, A.: The Carbon-Capture Efficiency of Natural Water Alkalinization: Implications For Enhanced weathering, Science of The Total Environment, 838, 156524, https://doi.org/10.1016/j.scitotenv.2022.156524, 2022.

Bijma, J., Hagens, M., Hammes, J. S., Planavsky, N., Pogge von Strandmann, P. A. E., Reershemius, T., Reinhard, C. T., Renforth, P., Suhrhoff, T. J., Vicca, S., Vienne, A., and Wolf-Gladrow, D.: Reviews and syntheses: Carbon vs. cation based MRV of Enhanced Rock Weathering and the issue of soil organic carbon, Biogeosciences, 23, 53–75, https://doi.org/10.5194/bg-23-53-2026, 2026.

Boito, L., Steinwidder, L., Rijnders, J., Berwouts, J., Janse, S., Niron, H., Roussard, J., Vienne, A., and Vicca, S.: Enhanced Rock Weathering Altered Soil Organic Carbon Fluxes in a Plant Trial, Global Change Biology, 31, e70373, https://doi.org/10.1111/gcb.70373, 2025.

Brantley, S. L.: Understanding the Lab-Field Discrepancy in Mineral Dissolution From Flasks to Enhanced Rock Weathering, Reviews of Geophysics, 63, e2025RG000881, https://doi.org/10.1029/2025RG000881, 2025.

Buma, B., Dietzen, C., Gordon, D. R., Maher, K., Neumann, R. B., Planavsky, N. J., Reershemius, T., Suhrhoff, T. J., Vicca, S., Waring, B. G., Almaraz, M., Calabrese, S., Derry, L. A., Morgan, M. G., Higgins, J., Houlton, B. Z., Kanzaki, Y., Klemme, A., Kukla, T., Oldfield, E. E., Power, I. M., Pearce, C. R., Silver, W. L., and Zhang, S.: Expert elicitation on agricultural enhanced weathering reveals carbon dioxide removal potential and uncertainties in loss pathways, Commun Earth Environ, https://doi.org/10.1038/s43247-026-03375-5, 2026.

Calabrese, S., Wild, B., Bertagni, M. B., Bourg, I. C., White, C., Aburto, F., Cipolla, G., Noto, L. V., and Porporato, A.: Nano- to Global-Scale Uncertainties in Terrestrial Enhanced Weathering, Environmental Science & Technology, 12, 2021.

Cambardella, C. A. and Elliott, E. T.: Particulate Soil Organic-Matter Changes across a Grassland Cultivation Sequence, Soil Science Soc of Amer J, 56, 777–783, https://doi.org/10.2136/sssaj1992.03615995005600030017x, 1992.

Carignan, J., Hild, P., Mevelle, G., Morel, J., and Yeghicheyan, D.: Routine Analyses of Trace Elements in Geological Samples using Flow Injection and Low Pressure On-Line Liquid Chromatography Coupled to ICP-MS: A Study of Geochemical Reference Materials BR, DR-N, UB-N, AN-G and GH, Geostandards and Geoanalytical Research, 25, 187–198, https://doi.org/10.1111/j.1751-908X.2001.tb00595.x, 2001.

Carstensen, J., Reducha Andersen, N., Christensen, J. & Mohn, C. (2021). *Havets pH-balance – påvirkning fra klima og næringsstoffer*. Aarhus University, DCE – Danish Centre for Environment and Energy, Scientific Report No. 429, 76 pp.

Clarkson, M. O., Larkin, C. S., Swoboda, P., Reershemius, T., Suhrhoff, T. J., Maesano, C. N., and Campbell, J. S.: A review of measurement for quantification of carbon dioxide removal by enhanced weathering in soil, Front. Clim., 6, https://doi.org/10.3389/fclim.2024.1345224, 2024.

Danmarks Miljøportal. *Kemidata: Environmental monitoring data.* Available at: https://miljoedata.miljoeportal.dk/ (accessed September 2026).

Dietzen, C. and Rosing, M. T.: Quantification of CO2 uptake by enhanced weathering of silicate minerals applied to acidic soils, International Journal of Greenhouse Gas Control, 125, 103872, https://doi.org/10.1016/j.ijggc.2023.103872, 2023.

Dietzen, C., Gunnarsen, K. C., Jensen, L. S., and Rosing, M. T.: Glacial Rock Flour Field Trial: Vojens, Denmark [Data set], University of Copenhagen, https://doi.org/10.17894/UCPH.16FBF798-6DE6-40D6-8437-E70CD0A42FC1, 2022.

Dietzen, C., Rizzi, M., Suhrhoff, T. J., and Rosing, M.: 5 year resampling of soil from Glacial Rock Flour Field trial in Vojens DK: Data and code for analysis, https://doi.org/10.17894/ucph.63ae53e9-9269-4021-8f25-084dcbdf9459, 2026.

DMI: Vejrarkiv, http://www.dmi.dk/vejrarkiv/, last access: 18 March 2026., 2026.

Dupla, X., Bertagni, M. B., and Grand, S.: Three Years of Field Trials Indicate a Sustained Enhanced Rock Weathering Signal with Limited CO_2 Removal, Environ. Sci. Technol., 59, 25751–25764, https://doi.org/10.1021/acs.est.5c09820, 2025.

Duque, C., Nilsson, B., and Engesgaard, P.: Groundwater–surface water interaction in Denmark, WIREs Water, 10, e1664, https://doi.org/10.1002/wat2.1664, 2023.

Edwards, D. P., Lim, F., James, R. H., Pearce, C. R., Scholes, J., Freckleton, R. P., Beerling, D. J., and Edwards, D. P.: Climate change mitigation : potential benefits and pitfalls of enhanced rock weathering in tropical agriculture, Biology Letters, 13, https://doi.org/10.1098/rsbl.2016.0715, 2017.

Elberling, B. and Matthiesen, H.: Methodologically controlled variations in laboratory and field pH measurements in waterlogged soils, European Journal of Soil Science, 58, 207–214, https://doi.org/10.1111/j.1365-2389.2006.00828.x, 2007.

Fang, Q., Lu, A., Hong, H., Kuzyakov, Y., Algeo, T. J., Zhao, L., Olshansky, Y., Moravec, B., Barrientes, D. M., and Chorover, J.: Mineral weathering is linked to microbial priming in the critical zone, Nat Commun, 14, 345, https://doi.org/10.1038/s41467-022-35671-x, 2023.

Georgiou, K., Jackson, R. B., Vindušková, O., Abramoff, R. Z., Ahlström, A., Feng, W., Harden, J. W., Pellegrini, A. F. A., Polley, H. W., Soong, J. L., Riley, W. J., and Torn, M. S.: Global stocks and capacity of mineral-associated soil organic carbon, Nat Commun, 13, 3797, https://doi.org/10.1038/s41467-022-31540-9, 2022.

Georgiou, K., Angers, D., Champiny, R. E., Cotrufo, M. F., Craig, M. E., Doetterl, S., Grandy, A. S., Lavallee, J. M., Lin, Y., Lugato, E., Poeplau, C., Rocci, K. S., Schweizer, S. A., Six, J., and Wieder, W. R.: Soil Carbon Saturation: What Do We Really Know?, Glob Chang Biol, 31, e70197, https://doi.org/10.1111/gcb.70197, 2025.

GEUS: Surface Geology Map of Denmark 1:25.000, https://eng.geus.dk/products-services-facilities/data-and-maps/maps-of-denmark, last access: 3 November 2022, 2020., 2020.

Gunnarsen, K. C., Jensen, L. S., Rosing, M. T., and Dietzen, C.: Greenlandic Glacial Rock Flour Improves Crop Yield in Organic Agricultural Production, Nutrient Cycling in Agroecosystems, 2023.

Harbo, L. S., Olesen, J. E., Liang, Z., Christensen, B. T., and Elsgaard, L.: Estimating organic carbon stocks of mineral soils in Denmark: Impact of bulk density and content of rock fragments, Geoderma Regional, 30, e00560, https://doi.org/10.1016/j.geodrs.2022.e00560, 2022.

Hartmann, J., West, A. J., Renforth, P., Köhler, P., De La Rocha, C. L., Wolf-gladrow, D. A., Dürr, H. H., Scheffran, J., Rocha, C. L. D. L., Wolf-gladrow, D. A., Dürr, H. H., Scheffran, J., De La Rocha, C. L., Wolf-gladrow, D. A., Dürr, H. H., and Scheffran, J.: Enhanced chemical weathering as a geoengineering strategy to reduce atmospheric carbon dioxide, supply nutrients, and mitigate ocean acidification, Reviews of Geophysics, 51, 113–149, https://doi.org/10.1002/rog.20004, 2013.

Holden, F., Davies, K., Bird, M., Hume, R., Green, H., Beerling, D., and Nelson, P.: In-field carbon dioxide removal via weathering of crushed basalt applied to acidic tropical agricultural soil, Science of The Total Environment, 955, 176568, https://doi.org/10.1016/j.scitotenv.2024.176568, 2024.

Huang, J. and Hartemink, A. E.: Soil and environmental issues in sandy soils, Earth-Science Reviews, 208, 103295, https://doi.org/10.1016/j.earscirev.2020.103295, 2020.

Kantola, I. B., Blanc-Betes, E., Masters, M. D., Chang, E., Marklein, A., Moore, C. E., von Haden, A., Bernacchi, C. J., Wolf, A., Epihov, D. Z., Beerling, D. J., and DeLucia, E. H.: Improved net carbon budgets in the US Midwest through direct measured impacts of enhanced weathering, Global Change Biology, 29, 7012–7028, https://doi.org/10.1111/gcb.16903, 2023.

Kanzaki, Y., Planavsky, N. J., and Reinhard, C. T.: New estimates of the storage permanence and ocean co-benefits of enhanced rock weathering, PNAS Nexus, 2, pgad059, https://doi.org/10.1093/pnasnexus/pgad059, 2023.

Kelland, M. E., Wade, P. W., Lewis, A. L., Taylor, L. L., Sarkar, B., Andrews, M. G., Lomas, M. R., Cotton, T. E. A. E. A., Kemp, S. J., James, R. H., Pearce, C. R., Hartley, S. E., Hodson, M. E., Leake, J. R., Banwart, S. A., Beerling, D. J., Wade, P. W., Johnson, D. A., Lewis, A. L., Andrews, M. G., Lomas, M. R., Cotton, T. E. A. E. A., Kemp, S. J., Taylor, L. L., James, R. H., Pearce, C. R., Hartley, S. E., Hodson, M. E., Leake, J. R., Banwart, S. A., Beerling, D. J., Sarkar, B., Andrews, M. G., Lomas, M. R., Cotton, T. E. A. E. A., Kemp, S. J., James, R. H., Pearce, C. R., Hartley, S. E., Hodson, M. E., Leake, J. R., Banwart, S. A., and Beerling, D. J.: Increased yield and CO2 sequestration potential with the C4 cereal Sorghum bicolor cultivated in basaltic rock dust-amended agricultural soil, Global Change Biology, 26, 3658–3676, https://doi.org/10.1111/gcb.15089, 2020.

Kleber, M., Bourg, I. C., Coward, E. K., Hansel, C. M., Myneni, S. C. B., and Nunan, N.: Dynamic interactions at the mineral–organic matter interface, Nat Rev Earth Environ, 2, 402–421, https://doi.org/10.1038/s43017-021-00162-y, 2021.

Köhler, P., Hartmann, J., and Wolf-Gladrow, D. A.: Geoengineering potential of artificially enhanced silicate weathering of olivine., Proceedings of the National Academy of Sciences of the United States of America, 107, 20228–20233, https://doi.org/10.1073/pnas.1000545107, 2010.

Larkin, C. S., Andrews, M. G., Pearce, C. R., Yeong, K. L., Beerling, D. J., Bellamy, J., Benedick, S., Freckleton, R. P., Goring-Harford, H., Sadekar, S., and James, R. H.: Quantification of CO2 removal in a large-scale enhanced weathering field trial on an oil palm plantation in Sabah, Malaysia, Front. Clim., 4, https://doi.org/10.3389/fclim.2022.959229, 2022.

Lenth, R.: emmeans: Estimated Margina Means, aka Least-Squares Means. (1.7.2.), https://CRAN.R-project.org/package=emmeans, 2022.

Lopez-Sangil, L. and Rovira, P.: Sequential chemical extractions of the mineral-associated soil organic matter: An integrated approach for the fractionation of organo-mineral complexes, Soil Biology and Biochemistry, 62, 57–67, https://doi.org/10.1016/j.soilbio.2013.03.004, 2013.

Matthiesen, H.: In situ measurement of soil pH, Journal of Archaeological Science, 31, 1373–1381, https://doi.org/10.1016/j.jas.2004.03.005, 2004.

Niron, H., Vienne, A., Frings, P., Poetra, R., and Vicca, S.: Exploring the synergy of enhanced weathering and Bacillus subtilis: A promising strategy for sustainable agriculture, Global Change Biology, 30, e17511, https://doi.org/10.1111/gcb.17511, 2024.

Obour, P. B., Dietzen, C., Oppong Danso, E., Arthur, E., Adu, M. O., and Rosing, M. T.: Limited short-term benefits of glacial rock flour for enhancing the physical quality of tropical arable soils, European Journal of Soil Science, 75, e70028, https://doi.org/10.1111/ejss.70028, 2024.

Oppong Danso, E., Dietzen, C., Arthur, E., and Rosing, M. T.: Enduring increases in maize yield are a co-benefit of enhanced weathering of Greenlandic glacial rock flour in Ghana, Nutr Cycl Agroecosyst, 131, 761–772, https://doi.org/10.1007/s10705-025-10442-4, 2025.

Paradelo, R., Virto, I., and Chenu, C.: Agriculture, Ecosystems and Environment Net effect of liming on soil organic carbon stocks: A review, Agriculture, Ecosystems and Environment, 202, 98–107, https://doi.org/10.1016/j.agee.2015.01.005, 2015.

te Pas, E. E. E. M., Hagens, M., and Comans, R. N. J.: Assessment of the enhanced weathering potential of different silicate minerals to improve soil quality and sequester CO2, Frontiers in Climate, 4, 954064, https://doi.org/10.3389/fclim.2022.954064, 2023.

Pinheiro, J., Bates, D., DebRoy, S., Sarkar, D., and R Core Team: nlme: Linear and Nonlinear Mixed Effects Models, 2017.

Power, I. M., Hatten, V. N. J., Guo, M., Schaffer, Z. R., Rausis, K., and Klyn-Hesselink, H.: Are enhanced rock weathering rates overestimated? A few geochemical and mineralogical pitfalls, Front. Clim., 6, https://doi.org/10.3389/fclim.2024.1510747, 2025.

R Core Team: R: A Language and Environment for Statistical Computing, https://www.R-project.org/, 2023.

Ramos, E. J., Larsen, W. J., Hou, Y., Muñoz, S., Kemeny, P. C., Scheingross, J. S., Repasch, M. N., Hovius, N., Sachse, D., Ibarra, D. E., and Torres, M. A.: Competition or collaboration: Clay formation sets the relationship between silicate weathering and organic carbon burial in soil, Earth and Planetary Science Letters, 628, 118584, https://doi.org/10.1016/j.epsl.2024.118584, 2024.

Reershemius, T., Kelland, M. E., Jordan, J. S., Davis, I. R., D'Ascanio, R., Kalderon-Asael, B., Asael, D., Suhrhoff, T. J., Epihov, D. Z., Beerling, D. J., Reinhard, C. T., and Planavsky, N. J.: Initial Validation of a Soil-Based Mass-Balance Approach for Empirical Monitoring of Enhanced Rock Weathering Rates, Environ. Sci. Technol., https://doi.org/10.1021/acs.est.3c03609, 2023.

Renforth, P. and Henderson, G.: Assessing ocean alkalinity for carbon sequestration, Reviews of Geophysics, 55, 636–674, https://doi.org/10.1002/2016RG000533, 2017.

Rogers, B. and Maher, K.: An uncertainty-aware framework for solid-phase measurement and verification of enhanced weathering, Front. Clim., 7, https://doi.org/10.3389/fclim.2025.1688361, 2026.

Sakin, E.: Organic carbon organic matter and bulk density relationships in arid-semi arid soils in Southeast Anatolia region, AFRICAN JOURNAL OF BIOTECHNOLOGY, 11, https://doi.org/10.5897/AJB11.2297, 2012.

Sanderman, J., Fillery, I. R. P., Jongepier, R., Massalsky, A., Roper, M. M., Macdonald, L. M., Maddern, T., Murphy, D. V., and Baldock, J. A.: Carbon sequestration under subtropical perennial pastures II: Carbon dynamics, Soil Research, 51, 771–780, https://doi.org/10.1071/SR12351, 2013.

Sarkar, S. R.: Glacial Rock Flour: its Characteristics and Enhanced Weathering, PhD Thesis, University of Copenhagen, 2021.

Six, J., Conant, R. T., Paul, E. A., and Paustian, K.: Stabilization mechanisms of soil organic matter: Implications for C-saturation of soils, Plant and Soil, 241, 155–176, https://doi.org/10.1023/A:1016125726789, 2002.

Slessarev, E. W., Chadwick, O. A., Sokol, N. W., Nuccio, E. E., and Pett-Ridge, J.: Rock weathering controls the potential for soil carbon storage at a continental scale, Biogeochemistry, 157, 1–13, https://doi.org/10.1007/s10533-021-00859-8, 2022.

Sohng, J., Sokol, N. W., Whiteaker, S., Schmidt, R., Holzer, I., Goertzen, H., Peña, J., Houlton, B. Z., Montañez, I., O'Geen, A., and Scow, K.: Combining organic amendments with enhanced rock weathering shifts soil carbon storage in croplands, Science of The Total Environment, 998, 180179, https://doi.org/10.1016/j.scitotenv.2025.180179, 2025.

Sokol, N. W., Sohng, J., Moreland, K., Slessarev, E., Goertzen, H., Schmidt, R., Samaddar, S., Holzer, I., Almaraz, M., Geoghegan, E., Houlton, B., Montañez, I., Pett-Ridge, J., and Scow, K.: Reduced accrual of mineral-associated organic matter after two years of enhanced rock weathering in cropland soils, though no net losses of soil organic carbon, Biogeochemistry, 167, 989–1005, https://doi.org/10.1007/s10533-024-01160-0, 2024.

Statistics Denmark: Cropland, https://www.dst.dk/en/Statistik/emner/erhvervsliv/landbrug-gartneri-og-skovbrug/det-dyrkede-areal, last access: 18 March 2026, 2025., 2025.

Steinwidder, L., Boito, L., Frings, P. J., Niron, H., Rijnders, J., de Schutter, A., Vienne, A., and Vicca, S.: Beyond Inorganic C: Soil Organic C as a Key Pathway for Carbon Sequestration in Enhanced Weathering, Global Change Biology, 31, e70340, https://doi.org/10.1111/gcb.70340, 2025.

Styczen, M. and Sørensen, P. B.: Scenarios and Model Describing Fate and Transport of Pesticides in Surface Water for Danish Conditions, 63, Danish Environmental Protection Agency, 2004.

Suhrhoff, T. J., Reershemius, T., Wang, J., Jordan, J. S., Reinhard, C. T., and Planavsky, N. J.: A tool for assessing the sensitivity of soil-based approaches for quantifying enhanced weathering: a US case study, Front. Clim., 6, https://doi.org/10.3389/fclim.2024.1346117, 2024.

Suhrhoff, T. J., Reershemius, T., Jordan, J. S., Li, S., Zhang, S., Milliken, E., Kalderon-Asael, B., Ebert, Y., Nyateka, R., Thompson, J. T., Reinhard, C. T., and Planavsky, N. J.: An Updated Framework and Signal-to-Noise Analysis of Soil Mass Balance Approaches for Quantifying Enhanced Weathering on Managed Lands, Environ. Sci. Technol., acs.est.5c08303, https://doi.org/10.1021/acs.est.5c08303, 2025.

Suhrhoff, T. J., Dietzen, C., Kukla, T., Lunstrum, A., Reershemius, T., Thompson, J. T., Almaraz, M., Bertagni, M. B., Bullock, L. A., D'Ascanio, R., Falkson, I., Frings, P., Gregg, R., Iff, N., Lambert, J., Li, Y., Rogers, B., Schneider, J. M., Swanson, E. H., Tao, F., Tsao, S. S.-E., Bauwhede, R. V. D., Zhang, S., Anand, S. K., Campbell, J., Chiaravalloti, I., Davis, I., Dobson,

765 M., Dupla, X., Foteinis, S., Guo, M., Harrington, K., Kent, C., Klemme, A., Kroeger, J., Linke, T., Linnekogel, S., Moller, S.,
766 Milliken, E., Ndlovu, L., Niron, H., Patel, S., Pihlap, E., Rees, K., Rioux, R., Rizzi, M., Shaheen, S., Steinwidder, L., Steeley,
767 I., Sweere, T., Sun, F., Sun, X., Tatge, W., Lemus, L. T., Vienne, A., Westphalen, J., Woollen, B. J., Baum, C. M., Brantley,
768 S., Calabrese, S., Cyronak, T., Dorndorf, T., Fyson, C., Hagens, M., Hartmann, J., Holzer, I., Houlton, B., James, R., Jensen,
769 K., Kanzaki, Y., Khan, A., Levy, C., Lueck, S., Manning, D., Manning, J. R. H., Drewer, J. M. zu, Neumann, R. B., Pearce,
770 C., Strandmann, P. P. von, Power, I. M., Raymond, P. A., Renforth, P., Repke, T., Saiers, J. E., Santos, R., Smolen, J., Tan,
771 L., Vicca, S., Vorrath, M.-E., Webb, R., Yao, Y., Zhang, B., Reinhard, C., Planavsky, N., and Fuss, S.: An Ecosystem of
772 Carbon Dioxide Removal Reviews – Part 3: Enhanced Weathering, CDRXIV, 2026a.

773 Suhrhoff, T. J., Reinhard, C. T., Kanzaki, Y., Tsao, S. S.-E., Woollen, B., Reershemius, T., Shaheen, S., Saiers, J., Zhang, S.,
774 Raymond, P. A., and Planavsky, N. J.: Agricultural liming is a carbon sink in the Mississippi River Basin, Nature, 1–6,
775 https://doi.org/10.1038/s41586-026-11040-2, 2026b.

776 Tingey, S., Wadham, J. L., Telling, J., Flynn, S., Hawkings, J. R., Palinkas, S. S., Mun, Y., Yates, C. A., Lamarche-Gagnon,
777 G., Burford, R., Ramanathan, A. L., Hetherington, A., Dodd, A. N., Liu, X., and Sgouridis, F.: The potential for glacial flour
778 to impact soil fertility, crop yield and nutrition in mountain regions, iScience, 28, https://doi.org/10.1016/j.isci.2024.111476,
779 2025.

780 Vicca, S., Goll, D. S., Hagens, M., Hartmann, J., Janssens, I. A., Neubeck, A., Peñuelas, J., Poblador, S., Rijnders, J., Sardans,
781 J., Struyf, E., Swoboda, P., Groenigen, J. W., Vienne, A., and Verbruggen, E.: Is the climate change mitigation effect of
782 enhanced silicate weathering governed by biological processes?, Global Change Biology, 28, 711–726,
783 https://doi.org/10.1111/gcb.15993, 2022.

784 Vienne, A., Frings, P., Poblador, S., Steinwidder, L., Rijnders, J., Schoelynck, J., Vinduskova, O., and Vicca, S.: Earthworms
785 in an enhanced weathering mesocosm experiment: Effects on soil carbon sequestration, base cation exchange and soil CO2
786 efflux, Soil Biology and Biochemistry, 199, 109596, https://doi.org/10.1016/j.soilbio.2024.109596, 2024.

787 Wang, Y., Yao, Z., Zhan, Y., Zheng, X., Zhou, M., Yan, G., Wang, L., Werner, C., and Butterbach-Bahl, K.: Potential benefits
788 of liming to acid soils on climate change mitigation and food security, Global Change Biology, 27, 2807–2821,
789 https://doi.org/10.1111/gcb.15607, 2021.

790 Xu, T., Yuan, Z., Vicca, S., Goll, D. S., Li, G., Lin, L., Chen, H., Bi, B., Chen, Q., Li, C., Wang, X., Wang, C., Hao, Z., Fang,
791 Y., and Beerling, D. J.: Enhanced silicate weathering accelerates forest carbon sequestration by stimulating the soil mineral
792 carbon pump, Global Change Biology, 30, e17464, https://doi.org/10.1111/gcb.17464, 2024.

793 Xu, T., Li, H., Vicca, S., Goll, D. S., Beerling, D. J., Chen, Q., Bi, B., Yang, Z., Wang, X., and Yuan, Z.: Enhanced Rock
794 Weathering Promotes Soil Organic Carbon Accumulation: A Global Meta-Analysis Based on Experimental Evidence, Global
795 Change Biology, 31, e70483, https://doi.org/10.1111/gcb.70483, 2025.

796 Yu, W.: Where and why do particulate organic matter (POM) and mineral-associated organic matter (MAOM) differ among
797 diverse soils?, Soil Biology and Biochemistry, 2022.

798 Zhang, H.-M., Liang, Z., Li, Y., Chen, Z.-X., Zhang, J.-B., Cai, Z.-C., Elsgaard, L., Cheng, Y., Jan Van Groenigen, K., and
799 Abalos, D.: Liming modifies greenhouse gas fluxes from soils: A meta-analysis of biological drivers, Agriculture, Ecosystems
800 & Environment, 340, 108182, https://doi.org/10.1016/j.agee.2022.108182, 2022.

801 Zhang, S., Reinhard, C. T., Liu, S., Kanzaki, Y., and Planavsky, N. J.: A framework for modeling carbon loss from rivers
802 following terrestrial enhanced weathering, Environ. Res. Lett., 20, 024014, https://doi.org/10.1088/1748-9326/ada398, 2025.

803 Klimadatastyrelsen, https://hipdata.dk/, last access: 18 March 2026., 2026.

804